A correlated light and electron microscopy approach to study the subcellular localization of phosphorylated vimentin in human lung tissue

Christine Péchoux, Fabrice Antigny, Frédéric Perros

A correlated light and electron microscopy approach to study the subcellular localization of phosphorylated vimentin in human lung tissue

Christine Péchoux[a,b,*], Fabrice Antigny[c,d], and Frédéric Perros[e]

[a]Université Paris-Saclay, INRAE, AgroparisTech, GABI, Jouy-en-Josas, France
[b]MIMA2 Imaging Core Facility, Microscopie et Imagerie des Microorganismes, Animaux et Aliments, INRAE, Jouy-en-Josas, France
[c]Université Paris-Saclay, Faculté de Médecine, Le Kremlin-Bicêtre, France
[d]INSERM UMR_S 999 "Hypertension Pulmonaire: Physiopathologie et Innovation Thérapeutique," Hôpital Marie Lannelongue, Le Plessis-Robinson, France
[e]Laboratoire CarMeN, UMR INSERM U1060/INRA U1397, Université Claude Bernard Lyon 1, Bron, France
*Corresponding author: e-mail address: christine.longin@inrae.fr

Contents

Methods in Cell Biology
ISSN 0091-679X
https://doi.org/10.1016/bs.mcb.2024.02.034

Abstract

Correlative microscopy is an important approach for bridging the resolution gap between fluorescence light and electron microscopy. Here, we describe a fast and simple method for correlative immunofluorescence and immunogold labeling on the same section to elucidate the localization of phosphorylated vimentin (P-Vim), a robust feature of pulmonary vascular remodeling in cells of human lung small arteries. The lung is a complex, soft and difficult tissue to prepare for transmission electron microscopy (TEM). Detailing the molecular composition of small pulmonary arteries (<500 μm) would be of great significance for research and diagnostics. Using the classical methods of immunochemistry (either hydrophilic resin or thin cryosections), is difficult to locate small arteries for analysis by TEM. To address this problem and to observe the same structures by both light and electron microscopy, correlative microscopy is a reliable approach. Immunofluorescence enables us to know the distribution of P-Vim in cells but does not provide ultrastructural detail on its localization. Labeled structures selected by fluorescence microscope can be identified and further analyzed by TEM at high resolution. With our method, the morphology of the arteries is well preserved, enabling the localization of P-Vim inside pulmonary endothelial cells. By applying this approach, fluorescent signals can be directly correlated to the corresponding subcellular structures in areas of interest.

1. Introduction

The term "correlative light and electron microscopy" (CLEM) describes a wide range of approaches that combine complementary microscopy techniques to provide more information than one could get by applying only a single type of microscopy. Often, CLEM involves wide-field light/laser microscopy with subsequent electron microscopy (EM), using either transmission (TEM) or scanning electron microscopy (SEM) (Mironov & Beznoussenko, 2013). Light microscopy (LM) is used to study biological phenomena at a global scale, whereas EM is powerful at high resolution (Mironov & Beznoussenko, 2009). LM potentially allows a far bigger cell/tissue volume to be analyzed, since EM relies typically on ~80–100-nm thick sections, which are observed then at high magnification.

CLEM makes it possible to take advantage of the strengths both LM and EM. It allows the detection of target macromolecules in relatively large specimen volumes by LM. These target macromolecules are then re-located by EM, and this can also be combined with immuno-electron microscopy (iEM) by using colloidal gold particles (Sousa, Rodrigues Loios, Faisca, & Tranfield, 2020). Immuno-gold labeling allows a precise localization of antigenic sites without compromising the underlying ultrastructural findings.

Thus, detailed immunomorphological assessment is achieved. IEM techniques permit clarification of immunohistochemistry results by labeling antigenic epitopes in cases where LM immunochemistry fails to show unequivocal results. Ultrastructural labeling enables precise localization of the antigenic site detected, which is essential for accurate diagnosis in a given case, thus providing immunomorphological correlation. The specificity of the interpreted results can then be judged accordingly. Overall, ultrastructural immunolabeling is more sensitive than light microscopic immunocytochemistry (Herrara, 1992).

Expression of vimentin has been reported in a wide range of cell types, particularly in mesenchymal cells of connective tissue, the central nervous system and muscle, fibroblasts, activated endothelial cells, macrophages, neutrophils, and leukocytes (Larsson, Wilhelmsson, Pekna, & Pekny, 2004; Von Basserwitz et al., 1982). Under quiescent conditions, polymeric vimentin maintains cellular integrity, a physiological "traditional" role that, without vimentin, might be compensated for (or performed) by other intermediate filaments. Indeed, vimentin is not critical for the survival of mice under normal physiological conditions. Vimentin$^{-/-}$ mice are viable and do not have obvious phenotypes (Colucci-Guyon, Dunia, Paulin, Pournin, & Babinet, 1994; Eckes et al., 1998; Satelli & Li, 2011). However, under stress and stimulatory conditions, vimentin phosphorylation impairs the steady state of vimentin in favor of increased free depolymerized vimentin. This "activated" vimentin pool, in turn, mediates the "nontraditional" vimentin functions such as protection from apoptosis, promotion of cell proliferation and differentiation (i.e., an epithelial-to-mesenchymal transition). We already showed that vimentin phosphorylation is a robust feature of pulmonary vascular remodeling in pulmonary arterial hypertension (Ranchoux et al., 2015).

Most reports on immunolocalized vimentin in various normal arteries have indicated that this protein is widely distributed in vascular smooth muscle cells (Johansson, Eriksson, Virtanen, & Thornell, 1997). Fine-scale localization of vimentin or phospho-vimentin in the intima of small pulmonary vessels has traditionally been limited by the resolution of light microscopes, which is not powerful enough to identify the different labeled structures. Furthermore, the lung is a complex tissue and the localization of small arteries of interest in tissue samples is very difficult. Finding a small pulmonary artery directly by TEM is like looking for "a needle in a haystack". To illustrate this problem, the ratio between a histological sample and an EM section is shown in Fig. 1A (gray rectangle, lower left corner).

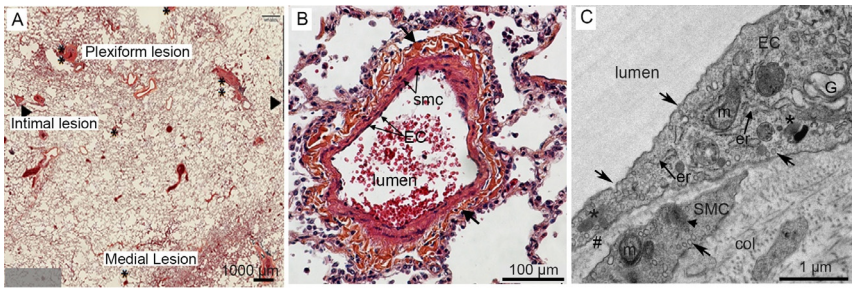

Fig. 1 PAH lesions and their distribution in lung tissue. (A) Histological image of a precapillary pulmonary arteries in pulmonary artery hypertension disease (PAH) with an increased medial thickness (medial lesions), eccentric or concentric intimal thickening (intimal lesions), and obliteration and recanalization of arteries (plexiform lesions). Such lesions represent only 1% of the human pulmonary tissue. The size of the tissue shown represents a tissue block (size $1.3 \times 1.6\,cm^2$), the gray rectangle (lower left corner) represents the block size ($0.1 \times 0.35\,cm^2$) as used for transmission electron microscopy (large arrow, intimal lesion; *, medial lesion; **, plexiform lesion) scale bar, 1000 µm. (B) Unaffected pulmonary artery. The lumen is surrounded by endothelial cells (EC) (small arrows) and the sub-endothelial smooth muscle cells (smc) are indicated by small arrows. The smooth muscle cell is surrounded by the intimal elastic lamina (large arrows) scale bar, 100 µm. (C) Ultrastructure of an endothelial cell and a smooth muscle cell. Electron microscopic image showing the unambiguous identification of organelles of both cell-types in lung tissue (Ranchoux et al., 2015). *Abbreviations*: EC, endothelial cell (small arrow); SMC, smooth muscle cell; col, collagen; G, Golgi apparatus; er, endoplasmic reticulum; m, mitochondria; caveolae, black arrows; Weibel-Palade bodies, *; basal membrane, #; scale bar, 1 µm.

Here, we describe an easy-to-use CLEM approach for the analysis of a "complicated" tissue like the lung. Our method allows to relocate a region of interest in a large histology section and use this selected region for further TEM analysis (Fig. 1B with histological features of a small pulmonary artery). In the following sections we give a step-by-step protocol for our developed CLEM approach.

2. Methods

2.1 Light microscopy

2.1.1 Chemical fixation

This step is crucial for a sufficient tissue preservation and impacts the following steps:

(a) gently inflate fresh lung tissue from PAH patients and healthy humans through the bronchi using an automated formalin-pump and immerse

samples in 0.1 M Sorensen Phosphate Buffer pH 7.4 (SPB) containing 10% formalin for 24 h

(b) fix lung samples of a size of 2 × 2.5 cm for 24 h in 4% formaldehyde in SPB at pH 7.4 solution under vacuum bell and agitation

(c) wash five times in SPB, 1 h each

(d) place the sample in increasing sucrose baths (10%, 2 × 40%) in SPB

(e) infiltrate the sample with sucrose for 1 day each bath under vacuum bell at 4 °C and agitation

(f) take the sample out of the sucrose solution and place it in cryostat molds (Fig. 2A)

(g) embed lung fragments with optimal cutting temperature (OCT)—medium and place the coated blocks for freezing at −80 °C

(h) cut thick (10–20 μm) sections of the frozen blocks at −30 °C (Fig. 2B–E) and collect the sections on correlative slides with patterns for sample recognition (Fig. 3)

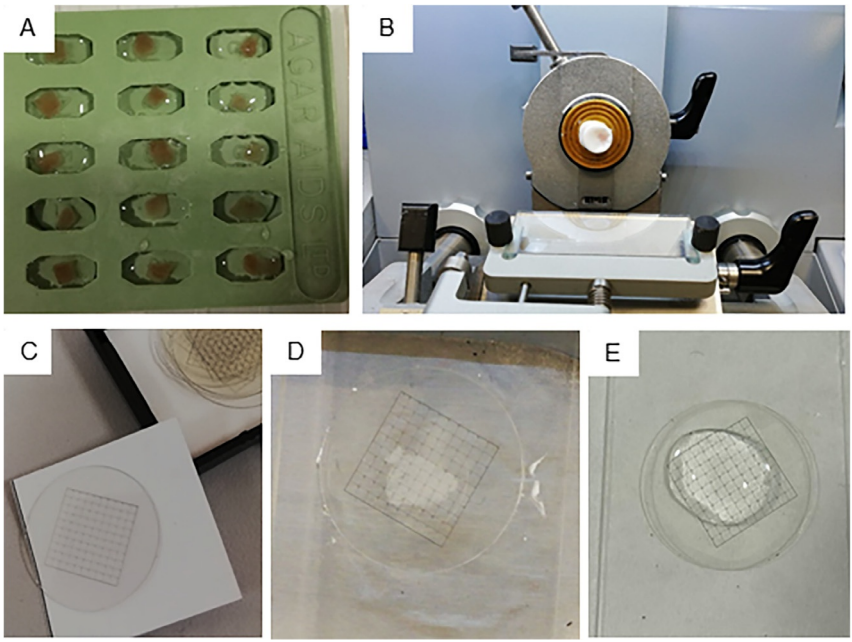

Fig. 2 Histological workflow. (A) Mold containing samples embedding in optimal cutting temperature (OCT) medium before freezing. (B) Sectioning using a cryostat. (C) Correlative slide with graduation. (D) Section picked up on a correlative slide and positioned on a glass slide. (E) Hydration of sections before staining with toluene blue.

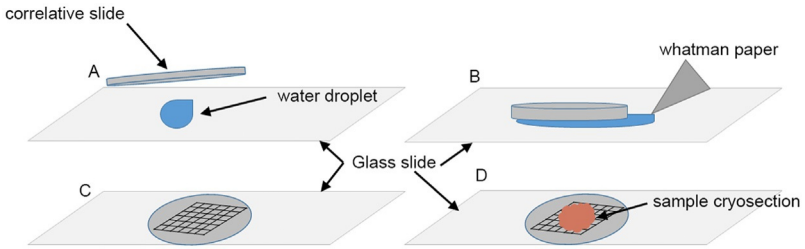

Fig. 3 Scheme 1 for the mounting of correlative slides on glass slides. (A) Water droplet on glass slide. (B) Removal of excess water. (C) Correlative slide for use on glass slide. (D) Cryo-section on correlative slide.

2.1.2 Immunofluorescence

The quality of the images will depend on the secondary antibodies chosen, to obtain good penetration of the probes. The unaltered areas in the sections are located in the middle of the sections.

A. Sample processing

The following steps are involved:

(a) quench sections with 0.5 M NH_4Cl pH 7.4 for 15 min at room temperature and rinse 3 × 10 min in SPB

(b) block sections in SPB containing 1% BSA, 0.5% Triton ×100, 10% goat serum and 10% human serum for 1 h

(c) incubate sections overnight at 4 °C with a primary mouse monoclonal antibody directed against phosphorylated-vimentin (1:50) in SPB containing 0.2% BSA, 0.2% Triton ×100 and 3% human serum; in parallel, incubate control sections without the primary antibody using the same buffer

(d) wash sections with 1% BSA-SPB, 3 × 10 min

(e) incubate sections for 1 h with a secondary goat anti-mouse antibody labeled with Alexa Fluor®594 FluoroNanoGold™-Fab′ (1:50)

(f) wash sections 3× for 10 min each step with SPB

(g) counterstain with DAPI (1:500) for 5 min

(h) wash sections 3× for 5 min in SPB

(i) mount the correlative slides turned upside down and mounted with prolong Gold (LifeTechnologies) in a glass bottom 35-mm cell culture dish (FluoroDish) (Figs. 4A and B and 5).

B. Data acquisition by confocal microscopy

Immunolabeled sections are imaged under an LSM 700 confocal microscope using 555 nm laser diodes. We use a 63× oil immersion objective

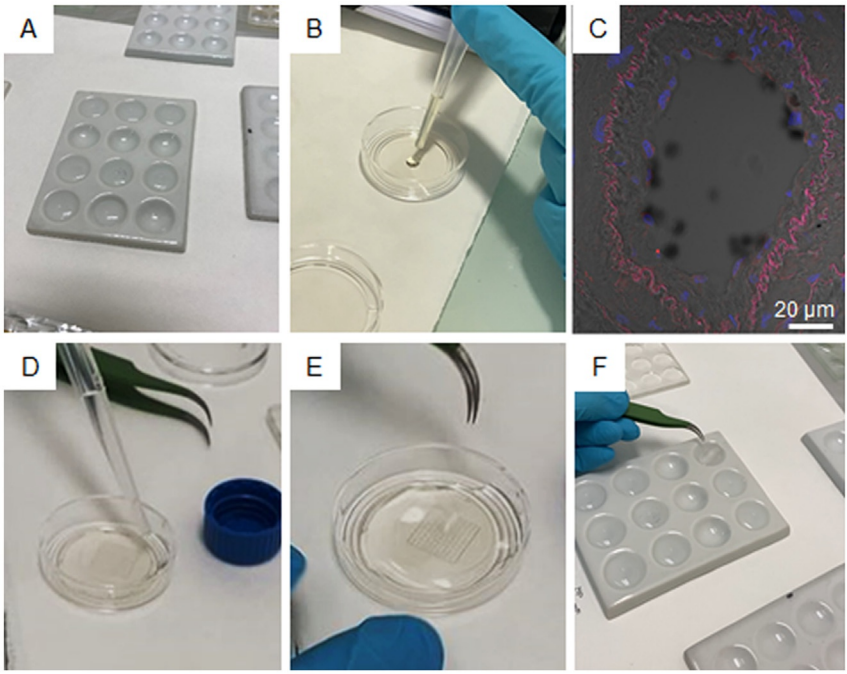

Fig. 4 Technique for mounting and removing the correlative slide. (A) Support for immunochemistry steps. (B) End of the process and addition of Prolong Gold drop at the bottom of a FluoroDish. (C) Typical focal plane image acquired by confocal microscopy after immunolabeling, scale bar, 20 µm. (D) FluoroDish petri filled with SPB. (E) Removal of the correlative slide. (F) Steps of dehydratation.

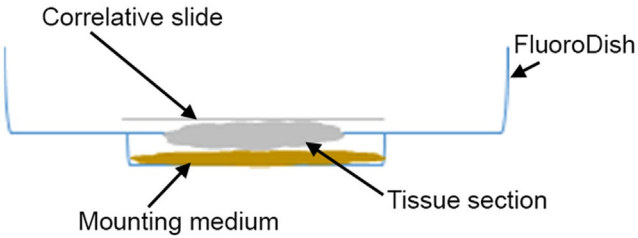

Fig. 5 Scheme 2: Mounting of the correlative slide in a FluoroDish. Use of FluoroDishes allowing an observation of the sections between the slide and a coverslip without any damage to the sample. FluoroDishes with a high-quality glass bottom. In combination with the mounting medium, this allows to acquire excellent high-magnification images with at high resolution.

(Zeiss, Plan-Apochromat, NA: 1.40) giving a resolution of 100 nm in the x, y planes and 300 nm along the z-axis. Optical sections are observed every 0.38 µm depth. Pulmonary arteries of interest are identified and localized using the grid numbers of the correlative slide. Images are recorded and processed using the ZEN software (Carl Zeiss) (Fig. 4C).

This process can be interrupted at the following steps: the cryostat sections can be kept in either the mounting medium or in PBS/SPB at +4 °C (Fig. 4D–F).

2.2 Electron microscopy

After data acquisition by confocal microscopy, areas of interest are identified using the coordinates from the correlative slides. The slides are conserved in SPB before EM processing.

2.2.1 Electron microscopy amplification processing

The amplification of nanogold particles with gold salts is a delicate process and must be carried out with the utmost care. The following steps have to be followed:

(a) fix selected thick cryo-sections with 1% glutaraldehyde in SPB for 5 min at room temperature and wash the sections for 5 min in SPB
(b) quench with 50 mM glycine and wash 3× with SPB before gold amplification (avoid interaction between the reagents)
(c) amplify the gold conjugates with one droplet of gold enhancement reagent (according to the manufacturer's recommendation) and apply the solution onto sections for 10 min (follow the amplification process under a binocular microscope)
(d) wash 3× with SPB
(e) stain sections with SPB containing 0.5% Oolong Tea Extract (OTE) for 30 min
(f) wash 3× with SPB
(g) post-fix with 0.5% osmium tetroxide containing 1.5% potassium cyanoferrate in 0.1 M SPB for 30 min
(h) wash slides 3× with double-distilled water
(i) dehydrate samples in a series of 50–90% ethanol for 5 min each step and finally by using 100% ethanol 3× for 5 min
(j) incubate samples in a 1:1100% ethanol/Epon (Embed 812) resin mix for 1 h
(k) infiltrate with pure Epon for 1 h

2.2.2 Electron microscopy embedding

Proceed by:

(a) pre-fill beam capsule with Epon
(b) using forceps, grab the correlative slide, flip it and position it on top of the beam capsule (with the sections facing the resin), take care to avoid air bubbles

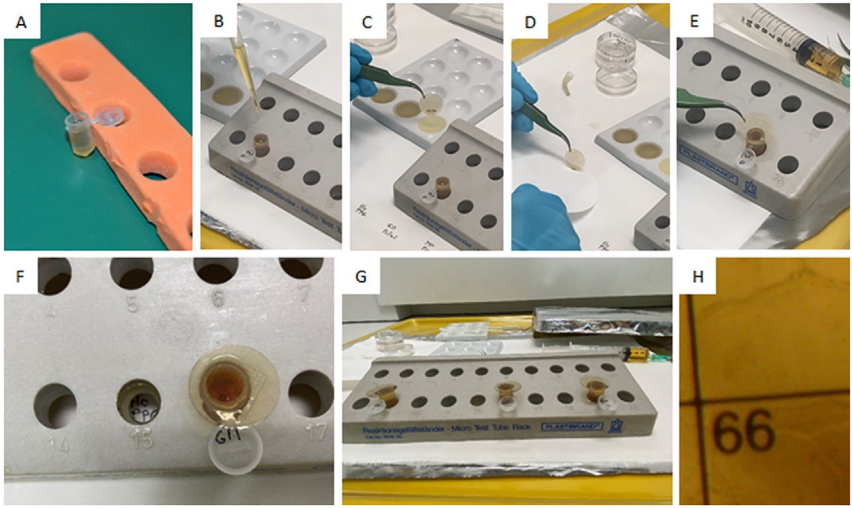

Fig. 6 Sample preparation for electron microscopy. (A) Beam capsule almost filled (2/3) with polymerized Epon 812. (B) Filling of the beam capsule with liquid Epon 812. (C–E) Use of forceps to position a correlative slide on top of the beam capsule with the sample side facing the resin (avoiding air bubbles at this stage is crucial). (F) Correlative slide on the top of beam capsules. (G) Samples after polymerization. (H) Landmark of the correlative slide as seen on the resin block.

(c) polymerize the resin in an oven at 60 °C for 24 h
(d) check the number in the grid of the area of interest under binocular microscope (Fig. 6H)

2.2.3 Ultramicrotomy and TEM

After resin embedding, areas of interest identified by confocal microscopy are sectioned to perform TEM:

(a) remove the plastic correlative slide using a razor blade (Fig. 7A–E)
(b) divide the block into at least two parts using a saw, thus increasing the number of samples for the TEM analysis (Fig. 7F–H)
(c) collect 500 nm-sections onto glass slides
(d) counterstain with methylene blue-azure II
(e) image sections with a light microscope (Fig. 7I)
(f) cut additional serial ultrathin (70 nm) sections by using an ultramicrotome (such as the Leica UC6) and collect the section on either 150/200 mesh or copper slot grids
(g) post-stain sections with Reynolds lead citrate for 3 min
(h) image grids using a TEM, acquire low-magnification pictures for tissue recognition (Fig. 7J) and high-magnification images to visualize the gold particles

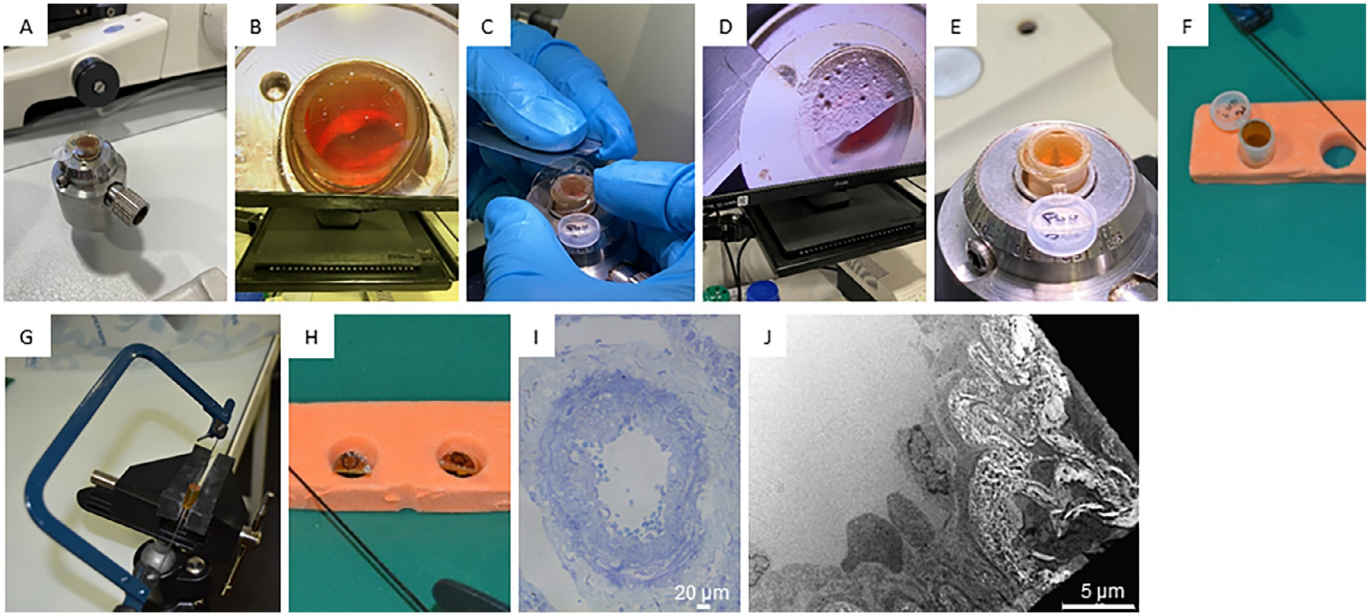

Fig. 7 Preparation of EM blocks for ultramicrotomy. (A–D) Removal of a correlative slide from the resin block using a razor blade. (E) Tissue sample visible at the surface of the beam capsule. (F) Resin block. (G) Use of a saw to cut resin block into pieces (to increase sample size). (H) Two resin samples of the same block. (I) Semi-thick section: scale bar, 20 µm. (J) Low-magnification TEM image: scale bar, 5 µm.

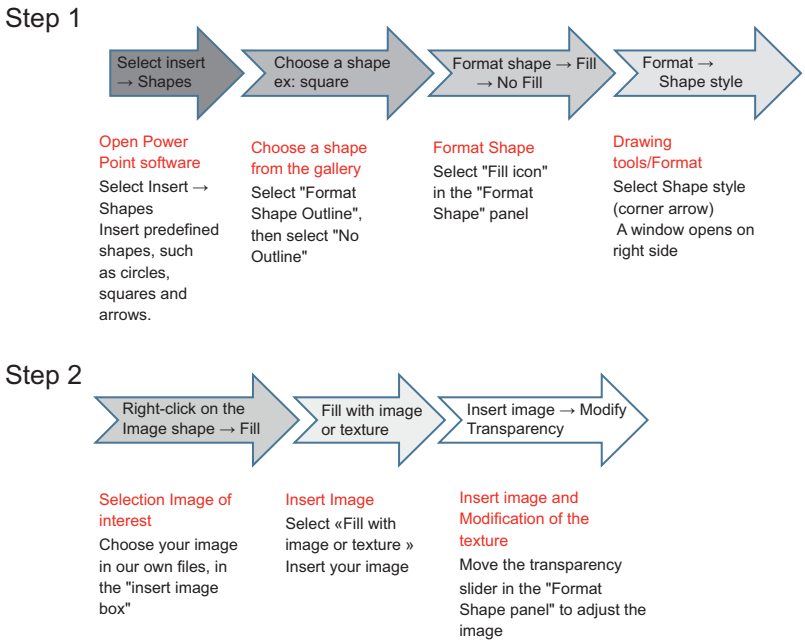

Fig. 8 Process for image overlay. Workflow on power point software used for correlation between light and electron microscopy images.

(i) align EM images obtained by TEM with LM images obtained following the immunofluorescence procedure

All electron microscope examinations are carried out by using a TEM operated at 80 kV (here a Hitachi HT7700 equipped with an AMT camera).

2.3 Image analysis

To correlate the obtained confocal and electron microscopy images, use ec-CLEM plugins of the ICY software package (Paul-Gilloteaux et al., 2017), or to overlay LM and EM images, use the transparisation process proposed by power point software (Fig. 8).

3. Instrumentation and materials

3.1 Light microscopy

Biological samples: Human lung samples from PAH patients and cancer patients (ctl). Protocol N8CO-08-003, ID RCB: 2008-A00485-50, approved on June 18, 2008, Lannelongue hospital, 133 av. de la Résistance, 92350 Le Plessis-Robinson, France.

3.1.1 Chemical fixation

Instrumentation:
- Fume-hood
- Automated pump (Microm Microtech, France)
- Stirring wheel at 4 °C
- Vacuum bell
- Freezer set at −80 °C
- Cryostat (Microm Microtech, France)

Materials:
- Dissection tools
- Pasteur pipettes
- Eppendorf tubes
- Cryostat molds
- Forceps
- Correlative slides with graticules (DeltaMicroscopie, France, #01ACMC35RND)

Reagents:
- Formalin 10%
- Formaldehyde 4% (15710, EMS)
- PBS (phosphate buffered saline) 1× pH 7.4 or SPB (Sorensen Phosphate Buffer) 0.1 M pH 7.4
- Sucrose
- Optimal Cutting Temperature component (Tissue Tek)
- Toluidine Blue

3.1.2 Immunofluorescence

Instrumentation:
- LSM 700 confocal microscope (Zeiss)

Materials:
- Plastic pipettes
- Forceps
- FluoroDish (WPI, Hitchin, UK, #FD35-100)

Reagents:
- Sorensen Phosphate Buffer 0.1 M pH 7.4
- NH_4Cl 50 mM pH 7.4
- BSA (bovine serum albumin)
- Triton ×100
- Goat serum
- Human serum
- Monoclonal mouse anti-phospho vimentine (Abcam, clone 4A4 #Ab22651)

- Alexa Fluor®594 FNG™-Fab′ GAM 1.4 nm (Nanoprobes, LFG Distribution #7302)
- 4′,6′-Diamidino-2-phenylindole (DAPI, Molecular Probes, France)
- Prolong Gold mounting medium (Fischer Scientific #11539306)

3.2 Electron microscopy

3.2.1 Electron microscopy amplification processing

Instrumentation:
- Fume-hood

Materials:
- Plastic pipettes
- Eppendorf tubes

Reagents:
- Glutaraldehyde 25% (EMS #16220)
- Sodium Cacodylate powder (EMS #12300)
- Glycine (Sigma #G-6388)
- Sorensen Phosphate Buffer 0.1 M pH 7.4
- Enhancement Kit (GoldEnhance™ EM Nanoprobes, LFG Distribution #2113)
- Osmium tetroxide (EMS #19190)
- Potassium cyanoferrate (Sigma Aldrich, #P3289-100G)
- Oolong Tea Extract (OTE) (DeltaMicroscopie, France, #19900-10)
- Ethanol

3.2.2 Electron microscopy embedding

Instrumentation:
- Fume-hood
- Oven (60 °C)

Materials:
- Plastic pipettes
- Forceps
- Beam capsules

Reagents:
- Epon Kit 812 (EMS #14900)

3.2.3 Ultramicrotomy and TEM

Instrumentation:
- Light microscope
- UC6 Ultramicrotome (Leica Microsystems)
- Transmission Electron Microscope (Hitachi HT7700 equipped with an AMT camera)

Materials:
- Plastic pipettes
- Diamond knives 45° (Diatome, LGF, France)
- Forceps
- Glass slides
- Razor blades
- Palladium-copper 150 and 200 mesh grids (DeltaMicroscopie, France)
- Copper slot grids coated with Formvar/carbon (DeltaMicroscopie, France)
- Whatman ashless paper (Servilab #1440-090)
- Saw

Reagents:
- Lead citrate (Reynolds)
- Methylene blue (Sigma Aldrich #M-9140)
- Borax (Sigma Aldrich #71997)
- Azure II (EMS #11210)

3.3 Image analysis

Instrumentation:
- Individual PC

Software:
- Zen software, Zeiss
- AMT software, Hitachi
- Ec-CLEM plugins from ICY software
- Power point software (Windows)

4. Results and discussion

4.1 General considerations for CLEM on specific tissues

There are experimental situations in which the resolving power of the EM is required and correlative protocols are the only methods to answer scientific questions. This is true for tissues that are difficult to prepare (such as air-filled lung samples) or, for sample, in which it is time consuming to locate specific features by TEM (such as small arteries, glomeruli, etc.). These tissues should be treated first by applying histological processing (fixation, embedding, sectioning), possibly followed by immunolabeling (iEM) (Sousa et al., 2020). When IEM is necessary, the protocol for fixation and embedding must be adjusted to avoid destruction of the morphology tissue and the antigenicity of target structures.

4.2 Cryostat section preservation (LM)

The ultrastructure of the small artery was preserved despite exposure to a high sucrose gradient, freezing, and post-embedding process. Previous research has demonstrated that the choice of the fixative and the cryoprotectant is essential to protect the ultrastructure (Chat & Péchoux, 2009; Eldred, Zucker, Karten, & Yazulla, 1983). Sucrose is a commonly used cryoprotectant in cryo-ultramicrotomy for immunogold labeling of ultrathin sections (Cortese, Diaspro, & Tacchetti, 2009; Tokuyasu, 1973; Vicidomini et al., 2010). Here, the chosen fixative and the cryoprotectant allowed us to achieve high-quality results for both morphology and labeling, despite a Triton x100 treatment. Morphologically, endothelial cells (EC) and smooth muscle cells (SMC) in the arterial wall resembled the structures described by Townsley (2012) and Smith and Heath (1979). Fine details were preserved for TEM analysis, as we recognized structures such as Weibel-Palade bodies inside the endothelium cytoplasm, caveolae vesicles around the plasma membrane, focal condensation of myofibrils in SMC, junctions between EC (Townsley, 2012) and elastin fibrils in the extracellular matrix. The ultrastructural integrity of our fixed tissue supported the validity of our technique and gave us confidence also for an evaluation of the immuno-labeling part of our protocol (Fig. 1C).

4.3 Probes and accessibility of antigens

In our context, lung tissue is very fragile, so after the whole procedure the outermost part of the sections is somewhat damaged. To obtain interpretable images, we eliminate the first sections, which is why we prepare thick cryo sections (10–20 μm), leaving the central part well preserved. However, it is also necessary to fluorescently label thick sections. The use of a small Fab′ fragment is a response to this problem. FluoroNanoGold (FNG) with a gold nanoparticle of 1.4 nm in diameter grafted on a Fab′ fragment shows a very good penetration into tissues (Robinson, Takizawa, Vandré, & Burry, 1998). The used FNG (bifunctional immunoprobe FNG; Takizawa, Powell, Hainfeld, & Robinson, 2015) penetrated into the sections and had an excellent accessibility to the antigens. We showed that the fluorescence of an FNG-Fab′ probe is visible over the entire depth of a 20 μm section (Fig. 9; Robinson, Takizawa, & Vandré, 2000a, 2000b). Robinson, Takizawa, and Vandré (2000b) demonstrated the efficiency of ultrasmall immunogold probes. These smaller reagents enhanced the labeling efficiency

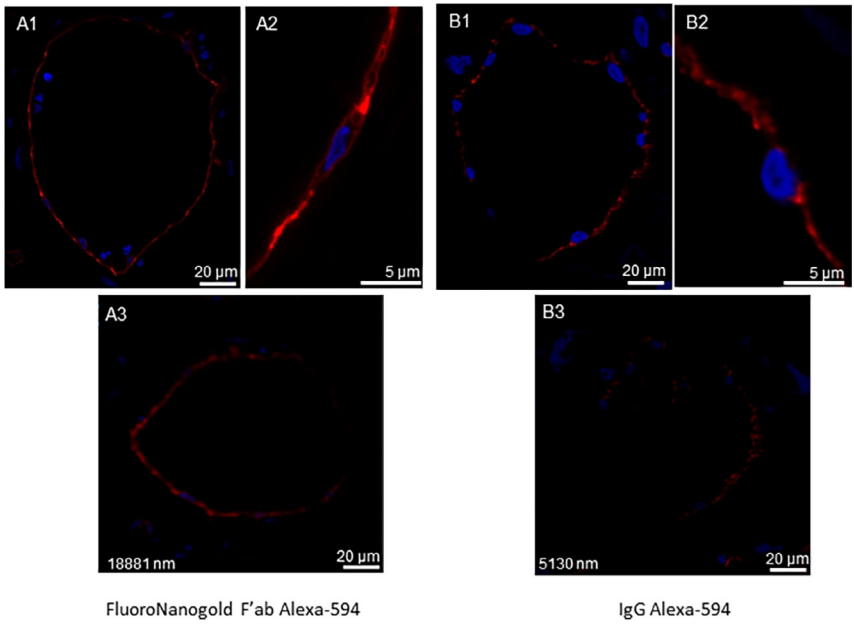

Fig. 9 Visualization of fluorescent probe penetration into thick cryosections. The FNG Alexa 594 Fab 1.4 nm gold-complex shows a more intense labeling (A1–A2) compared to IgG Alexa-594 (B1–B2). Penetration of the Fab-labeled probe (1.4 nm Fab for example), appeared greater than that of IgG-labeled probe. (A3) the use of a Fab-labeled probe maintains the signal over the entire thickness of the section (18 µm), whereas with an IgG-labeled probe on an adjacent section the signal is lost beyond a depth of 5 µm (B3). A1, A3, B1 and B3: scale bar, 20 µm. A2 and B2: scale bar: 5 µm.

and penetration. Small immunogold probes showed a higher labeling efficiency compared to larger probes.

4.4 Structural preservation for labeling

During a CLEM experiment, confocal acquisitions cannot be performed several times. Hence, the choice of coverslips and the mounting medium is essential to acquire high-quality images for further registration and/or alignment. To acquire images of sufficient quality by fluorescence microscopy and to prevent photo bleaching (Longin, Souchier, French, & Bryon, 1993; Takizawa & Robinson, 2000), we chose to use "Prolong Gold" medium to mount the coverslips, which considerably reduced fading, maintained gold particle stability (Takizawa & Robinson, 2000) and, therefore, it does not harden rapidly facilitating recovery of the coverslip. We also placed the correlative coverslip at the bottom of a FluoroDish-type Petri dish with a glass

bottom, thus enabling observations by using an invert confocal microscope. The use of Prolong Gold and FluoroDishes allowed us to acquire high-resolution images.

4.5 Probe amplification for electron microscopy

To prevent problems associated with an instability of the silver shell during OsO_4 post-fixation (Sawada & Esaki, 1994), we applied gold enhancement directly on FNG, without a step of silver enhancement before gold toning (Sawada & Esaki, 2000). Ultrasmall immunogold probes are the smallest immunogold reagents, thus yielding very good labeling efficiency and high-quality imaging in both LM and EM. By using gold enhancement rather than silver amplification (Hainfeld & Powell, 2000; Robinson et al., 2000a), we obtained particles that were regular in size and sufficiently separated to permit a semi-quantitative analysis. Silver enhancement is usually used for visualizing nanogold particles, but comes with a number of disadvantages: (I) The produced silver shell is unstable in OsO_4 and often becomes invisible after osmium tetroxide post-fixation (Sawada & Esaki, 2000), because OsO_4 acts on the silver aggregates and dissolved them. One of the best techniques is to reduce the concentration, contact time and temperature of OsO_4. Often, the silver shell is replaced with a more stable gold toning such as chloroauric acid to observe nanogold probes after OsO_4 post-fixation (Sawada & Esaki, 1994). (II) As described in their review (Baschong & Stierhof, 1998), there is often a problem arising with enhancement processing. Factors causing a lower reproducibility include pH and ionic strength. (III) The amplification kit for gold nanoparticles with gold toning (NanoProbes^{R}) limits the destructive action of OsO_4. However, we still recommend working at a concentration of 0.5% OsO_4 for 30 min.

4.6 Counterstaining of sections

In our procedure, we used Oolong Tea Extract (OTE) as a contrasting agent to replace uranyl acetate, which use is prohibited in many laboratories (Carpentier, Abreu, Trichet, & Satiat-Jeunemaitre, 2012; Kajikawa, Yamaguchi, Katsuda, & Miwa, 1975). OTE is recommended for staining connective tissue, specifically elastin fibers (Sato et al., 2003). Here, OTE allowed us to visualize our cell structures clearly, thus avoiding contamination caused by uranyl acetate deposits. OTE (particularly, polyphenolic compounds) penetrate the cell, and this results in good contrast with sharply

defined subcellular organelles and membrane (He & Liu, 2016). OsO_4 treatment after en-block OTE staining resulted in improved membrane contrast.

4.7 Data acquisition and correlation of LM and EM images

In confocal microscopy, the tissue is cut into optical sections along the z-axis. This allowed us to check the penetration of the antibody within the tissue and locate areas with intense labeling on the optical section. In this way, we could further evaluate at what depth in the section we had the strongest signal, which enabled us to go directly to the right level for EM sectioning. Thus, by using the axial planes for reference, we observed that phosphorylated vimentin was more strongly represented in EC lining the vessel lumen (Fig. 10A).

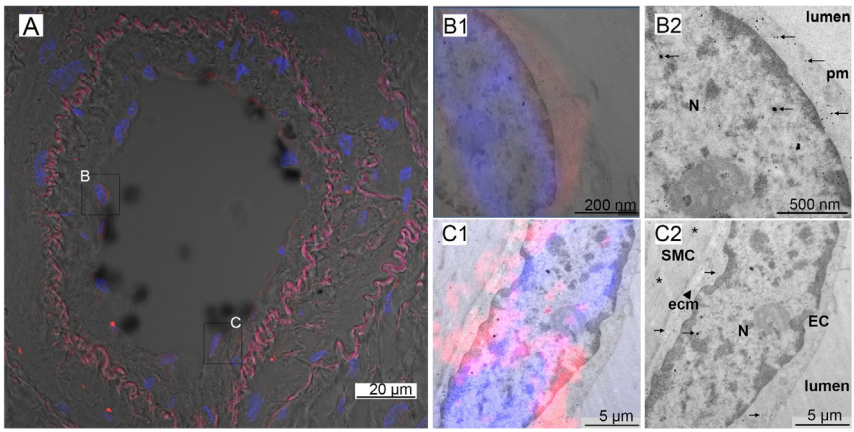

Fig. 10 Application of CLEM to visualize phospho-vimentin labeling in a PAH pulmonary artery. (A) Typical focal plane image of a pulmonary artery as acquired by confocal microscopy after P-Vim immunolabeling (red) and DAPI counterstaining (nuclei in blue). Two areas of interest, endothelial cells (B) and (C), were imaged by TEM. (B1) Overlay of confocal and TEM image showing the labeling in an endothelial cell as used for the imaging modalities (fluorescence label for light microscopy, gold particles for EM). (B2) Endothelial cell with P-Vim immunolabeling in the cytoplasm and the nucleus as points of variable diameter. Single gold particles and clusters are visible (black arrows). Image (B1) reveals strong fluorescence in the cytoplasm, while TEM image (B2) shows numerous gold particles distributed throughout the cytoplasm. (C1) Overlay of the fluorescent image and the TEM image of an endothelial cell, the red "spots" correspond to the labeling found on the image (C2) in the form of gold particle. (C2) Endothelial cell with weaker P-Vim immunolabeling. The labeling is visible as single gold particles (black arrows). Actin anchors are also visible in the SMC (asterisk). Abbreviations: pm, plasma membrane; N, nucleus; EC, endothelial cell; SMC, smooth muscle cell; ecm, extracellular matrix (arrowhead). Scale bar: A: 20 µm; B1: 200 nm; B2: 500 nm; C1 and C2: 5 µm. TEM images are acquired on MIMA2 facility: INRAE, 2018. Microscopy and Imaging Facility for Microbes, Animals and Foods. https://doi.org/10.15454/1.5572348210007727E12

The ultimate step in our protocol is the correlation of the LM and EM images. In our system, the confocal labeling is diffuse due to the need to use a high signal intensity for visualization. In addition, the autofluorescence of the internal elastic lamina, which surrounds the arteries, can masks the weak labeling of the phospho-vimentin. However, the labeling on the EM images shows many gold particles co-localized with the fluorescent labeling. The high quality of tissue preservation allows us to correlate the LM and EM images (Fig. 10B1 and C1). In TEM images obtained after gold amplification and sectioning, the cells were sufficiently preserved to identify intracellular structures in different cell types (Fig. 10B2 and C2). This enabled the identification of specific areas of interest.

5. Conclusion

The current procedure represents a complementary approach to pre-existing techniques (Agarwala et al., 2022; Bykov, Cortese, Briggs, & Bartenschlager, 2016). Our simple procedure described here permits to correlate light microscopic immunolabeling and electron microscopic observation with high precision. Using the same sample, immunolabeled signals can first be analyzed at the confocal microscopic level and then at the ultrastructural level. Regarding the required technical equipment, this can be performed in a non-CLEM-specialized lab as our approach does not require specific equipment for sample preparation and analysis.

Our method has proved its effectiveness and has been approved by its peers (Ranchoux et al., 2015). It has also been the subject of training, enabling it to be accessed and disseminated to a wider community, an idea supported in the preface by Müller-Reichert and Verkade (2021).

Acknowledgments

The authors acknowledge Martine Letheule (MIMA2 Facility) for technical support, Claire Boulogne (Imagery Gif Facility) for help in optimizing our approach experiments, and Claire Szczepaniak (UCA Facility) for photographic documentation. We are grateful to Dr. Lindsay Higgins for English corrections, Vlad Costache and Wendy Brand-Williams for their valuable comments. C.P. would like to have a very special thought for the colleague and friend Catherine Rucker-Martin, who is at the origin of this beautiful story. This work was supported by the French ANR (ANR-20-CE14-0006-01 to Frédéric Perros).

References

Agarwala, S., Kim, K. Y., Phan, S., Ju, S., Kong, Y. E., Castillon, G. A., et al. (2022). Defining the ultrastructure of the hematopoietic stem cell niche by correlative light and electron microscopy. *eLife*, *9*(11), e64835. https://doi.org/10.7554/eLife.64835. PMID: 35943143. PMCID: PMC9391045.

Baschong, W., & Stierhof, Y. D. (1998). Preparation, use, and enlargement of ultrasmall gold particles in immunoelectron microscopy. *Microscopy Research and Technique*, *42*(1), 66–79.

Bykov, Y. S., Cortese, M., Briggs, J. A., & Bartenschlager, R. (2016). Correlative light and electron microscopy methods for the study of virus-cell interactions. *FEBS Letters*, *590*(13), 1877–1895. https://doi.org/10.1002/1873-3468.12153. Epub 2016 Apr 13 PMID: 27008928.

Carpentier, A., Abreu, S., Trichet, M., & Satiat-Jeunemaitre, B. (2012). Microwaves and tea: New tools to process plant tissue for transmission electron microscopy. *Journal of Microscopy*, *247*(1), 94–105. https://doi.org/10.1111/j.1365-2818.2012.03626.x.

Chat, S., & Péchoux, C. (2009). Impact des procédures de fixation et de congélation sur la préservation du tissu de la glande mammaire de souris. *Cahier des Techniques de l'Inra*, *65*, 5–12.

Colucci-Guyon, E., Portier, M.-M., Dunia, I., Paulin, D., Pournin, S., & Babinet, C. (1994). Mice lacking vimentin develop and reproduce without an obvious phenotype. *Cell*, *79*(4), 679–694. https://doi.org/10.1016/0092-8674(94)90553-3. PMID: 7954832.

Cortese, K., Diaspro, A., & Tacchetti, C. (2009). Advanced correlative light/electron microscopy: Current methods and new developments using Tokuyasu cryosections. *Journal of Histochemistry and Cytochemistry*, *57*(12), 1103–1112.

Eckes, B., Dogic, D., Colucci-Guyon, E., Wang, N., Maniotis, A., Ingber, D., et al. (1998). Impaired mechanical stability, migration and contractile capacity in vimentin-deficient fibroblasts. *Journal of Cell Science*, *111*(13), 1897–1907. https://doi.org/10.1242/jcs.111.13.1897. PMID: 9625752.

Eldred, W. D., Zucker, C., Karten, H. J., & Yazulla, S. (1983). Comparison of fixation and penetration enhancement techniques for use in ultrastructural immunocytochemistry. *Journal of Histochemistry and Cytochemistry*, *31*(2), 285–292.

Hainfeld, J. F., & Powell, R. D. (2000). New frontiers in gold labeling. *Journal of Histochemistry and Cytochemistry*, *48*(4), 471–480.

He, X., & Liu, B. (2016). Oolong tea extract as a substitute for uranyl acetate in staining of ultrathin sections based on examples of animal tissues for transmission electron microscopy. *Journal of Microscopy*, *267*(1), 27–33. https://doi.org/10.1111/jmi.12544.

Herrera, G. A. (1992). Ultrastructural immunolabeling: A general overview of techniques and applications. *Ultrastructural Pathology*, *16*(1–2), 37–45. https://doi.org/10.3109/01913129209074548.

Johansson, B., Eriksson, A., Virtanen, I., & Thornell, L. E. (1997). Intermediate filament proteins in adult human arteries. *The Anatomical Record*, *247*(4), 439–448.

Kajikawa, K., Yamaguchi, T., Katsuda, S., & Miwa, A. (1975). An improved electron stain for elastic fibers using tannic acid. *Journal of Electron Microscopy*, *24*(4), 287–289.

Larsson, A., Wilhelmsson, U., Pekna, M., & Pekny, M. (2004). Increased cell proliferation and neurogenesis in the hippocampal dentate gyrus of old GFAP(−/−)Vim(−/−) mice. *Neurochemical Research*, *29*(11), 2069–2073. https://doi.org/10.1007/s11064-004-6880-2. PMID: 15662841.

Longin, A., Souchier, C., French, M. F., & Bryon, P. A. (1993). Comparison of anti-fading agents used in fluorescence microscopy: Image analysis and laser confocal microscopy study. *Journal of Histochemistry and Cytochemistry*, *41*(12), 1833–1840.

Mironov, A. A., & Beznoussenko, G. V. (2009). Correlative microscopy: A potent tool for the study of rare or unique cellular and tissue events. *Journal of Microscopy*, *235*(3), 308–321.

Mironov, A. A., & Beznoussenko, G. V. (2013). Correlative microscopy. *Methods in Cell Biology*, *113*, 209–255.

Müller-Reichert, T., & Verkade, P. (2021). In *Methods in cell biology—Correlative light and electron microscopy* (4th ed.). San Diego, CA: Elsevier Inc.

Paul-Gilloteaux, P., Heiligenstein, X., Belle, M., Domart, M.-C., Larijani, B., Collinson, L., et al. (2017). eC-CLEM: Flexible multidimensional registration software for correlative microscopies. *Nature Methods*, *14*(2), 102–103. https://doi.org/10.1038/nmeth.4170.

Ranchoux, B., Antigny, F., Rucker-Martin, C., Hautefort, A., Péchoux, C., Bogaard, H. J., et al. (2015). Endothelial-to-mesenchymal transition in pulmonary hypertension. *Circulation*, *131*(11), 1006–1018.

Robinson, J. M., Takizawa, T., & Vandré, D. D. (2000a). Enhanced labeling efficiency using ultrasmall immunogold probes: Immunocytochemistry. *Journal of Histochemistry and Cytochemistry*, *48*(4), 487–492.

Robinson, J. M., Takizawa, T., & Vandré, D. D. (2000b). Applications of gold cluster compounds in immunocytochemistry and correlative microscopy: Comparison with colloidal gold. *Journal of Microscopy*, *199*(3), 163–179.

Robinson, J. M., Takizawa, T., Vandré, D. D., & Burry, R. W. (1998). Ultrasmall immunogold particles: Important probes for immunocytochemistry. *Microscopy Research and Technique*, *42*(1), 13–23.

Satelli, A., & Li, S. (2011). Vimentin in cancer and its potential as a molecular target for cancer therapy. *Cellular and Molecular Life Sciences*, *68*(18), 3033–3046. https://doi.org/10.1007/s00018-011-0735-1. Epub 2011 Jun 3 PMID: 21637948. PMCID: PMC3162105.

Sato, S., Sasaki, Y., Adachi, A., Sai, W., Lui, X. L., & Namimatsu, S. (2003). Use of oolong tea extract (OTE) for elastin staining and enhancement in ultrathin sections. *Medical Electron Microscopy*, *36*(3), 179–182.

Sawada, H., & Esaki, M. (1994). Use of nanogold followed by silver enhancement and gold toning for preembedding immunolocalization in osmium-fixed, epon-embedded tissues. *Journal of Electron Microscopy*, *43*(6), 361–366.

Sawada, H., & Esaki, M. (2000). A practical technique to postfix nanogold-immunolabeled specimens with osmium and to embed them in epon for electron microscopy. *Journal of Histochemistry and Cytochemistry*, *48*(4), 493–498.

Smith, P., & Heath, D. (1979). Electron microscopy of the plexiform lesion. *Thorax*, *34*(2), 177–186.

Sousa, A. L., Rodrigues Loios, J., Faisca, P., & Tranfield, E. M. (2020). The Histo-CLEM workflow for tissues of model organisms. In T. Muller-Reichert, & P. Verkade (Eds.), *Methods in cell biology—Correlative light and electron microscopy* (4th ed., pp. 13–35). San Diego, CA: Elsevier Inc.

Takizawa, T., Powell, R. D., Hainfeld, J. F., & Robinson, J. M. (2015). FluoroNanogold: An important probe for correlative microscopy. *Journal of Chemical Biology*, *8*(4), 129–142.

Takizawa, T., & Robinson, J. M. (2000). Analysis of antiphotobleaching reagents for use with FluoroNanogold in correlative microscopy. *Journal of Histochemistry and Cytochemistry*, *48*(3), 433–436.

Tokuyasu, K. T. (1973). A technique for ultracryotomy of cell suspensions and tissues. *Journal of Cell Biology*, *57*(2), 551–565.

Townsley, M. I. (2012). Structure and composition of pulmonary arteries, capillaries, and veins. *Comprehensive Physiology*, *2*(1), 675–709.

Vicidomini, G., Gagliani, M. C., Cortese, K., Krieger, J., Buescher, P., Bianchini, P., et al. (2010). A novel approach for correlative light electron microscopy analysis. *Microscopy Research and Technique*, *73*(3), 215–224.

Von Bassewitz, D. B., Roessner, A., & Grundmann, E. (1982). Intermediate-sized filaments in cells of normal human colon mucosa, adenomas and carcinomas. *Pathology, Research and Practice*, *175*(2–3), 238–255. https://doi.org/10.1016/S0344-0338(82)80111-8. PMID: 6190147.